$_{y}Sn_{x}(Na,Tl)_{y}S$ [2], and indicates that the electron exchange between the centers of Sn^{2+} and Sn^{4+} is implemented using state of the valence band. In favor of such a mechanism is evidenced by the fact that the exchange is observed at low concentrations of tin, when the process can not be a direct exchange of electrons between the centers of the tin.

REFERENCES

1. *Anderson P. W.* Model for electronic structure of amorphous semiconductors // Physical Review Letters. 1975. V. 34. No 15. P. 953–955.

2. *Bordovsky G., Marchenko A.* and *Seregin P.* Mossbauer of Negative U Centers in Semiconductors and Superconductors. Identification, Properties, and Applicaton. Academic Publishing GmbH & Co. 2012. 499 p.

3. *Bordovskii G. A., Castro R. A., Marchenko A.V., Seregin P. P.* Thermal stability of tin charge states in the structure of the $(As_2Se_3)_{0.4}(SnSe)_{0.3}(GeSe)_{0.3}$ glass // Glass Physics and Chemistry. 2007. V. 33. No. 5. P. 467-470.

A. Shaldenkova, P. Seregin

CORRELATIONS OF THE ^{63}Cu NMR DATA WITH THE ^{67}Cu (^{67}Zn) AND THE ^{61}Cu (^{61}Ni) EMISSION MÖSSBAUER DATA FOR CERAMIC SUPERCONDUCTORS

A linear correlation between the quadrupole coupling constant C_{Cu} measured by the ^{63}Cu NMR technique on the one hand and the quadrupole coupling constants C_{Zn} and C_{Ni} measured by the ^{67}Cu(^{67}Zn) and ^{61}Cu(^{61}Ni) emission Mössbauer spectroscopy on the other hand has been found for ceramic superconductors.

Keywords: Mössbauer spectroscopy, NMR, electric field gradient.

А. В. Шалденкова, П. П. Серегин*

Победитель конкурса поддержки публикационной активности молодых исследователей (проект 3.1.2, ПСР РГПУ им. А. И. Герцена)

КОРРЕЛЯЦИОННЫЕ СООТНОШЕНИЯ МЕЖДУ ДАННЫМИ ЯМР ^{63}Cu И ЭМИССИОННОЙ МЕССБАУЭРОВСКОЙ СПЕКТРОСКОПИИ ^{67}Cu(^{67}Zn) И ^{61}Cu(^{61}Ni) ДЛЯ КЕРАМИЧЕСКИХ СВЕРХПРОВОДНИКОВ

Установлена линейная корреляция между постоянной квадрупольного расщепления C_{Cu}, измеренной методом ЯМР ^{63}Cu и постоянными квадрупольного расщепления C_{Zn} и C_{Ni},, измеренные методом эмиссионной мессбауэровской спектроскопии ^{67}Cu(^{67}Zn) и ^{61}Cu(^{61}Ni) для керамических сверхпроводников.

Ключевые слова: мессбауэровская спектроскопия, ЯКР, градиент электрического поля.

1. Introduction

One of the main problems in physics of high-temperature (high-T_c) superconductors is the determination of the spatial distribution of electronic defects in the lattices of copper metal oxides. A potentially effective method to solve this problem is to compare the experimentally determined and calculated parameters of the electric field gradient (EFG) tensor for specific lattice sites [2]. Copper sites are of utmost interest in such work because these atoms are found in the

composition of all high-T_c superconductors, and now it is considered as an established fact that superconductivity is activated along the Cu-O_2 planes.

Of all the methods used to determine the EFG at copper sites, special recognition is accorded nuclear magnetic resonance (NMR) using ^{63}Cu [1], along with ^{67}Cu(^{67}Zn) and ^{61}Cu(^{61}Ni) emission Mössbauer spectroscopy (EMS) [2]. The measurement results are presented in the form of parameters of the quadrupole interaction tensor the quadrupole interaction constant C= eQU_{zz} and the asymmetry parameter $\eta = \frac{U_{xx} - U_{yy}}{U_{zz}}$. Here Q is the quadrupole moment of the probe nucleus (Q =− 0.211 b for ^{63}Cu, Q = 0.17 b for ^{67}Zn, and Q = 0.162 b for ^{61}Ni), U_{xx}, U_{yy}, and U_{zz} are the components of the diagonalized EFG tensor at the probe nucleus, where $U_{xx} + U_{yy} + U_{zz} = 0$ and $|U_{xx}| < |U_{yy}| < |U_{zz}|$ and x, y, and z refer to the principal axes of the EFG tensor.

For the $^{63}Cu^{2+}$ and $^{61}Ni^{2+}$ probes EFG on nuclei is generated by lattice ions (crystal EFG) and by the aspherical valence shell of the probe atom (valence EFG); when the orientations of the principal axes of all the tensors coincide, the equation is

$$eQU_{zz} = eQ(1 - \gamma)\, V_{zz} + eQ(1 - R)\, W_{zz}, \quad (1)$$

where U_{zz}, V_{zz}, and W_{zz} are the principal components of the total, crystal, and valence EFG tensors for Cu and Ni , and γ and R are the Sternheimer coefficients for the Cu^{2+} and Ni^{2+} ions.

The situation is simplified when ^{67}Cu(^{67}Zn) EMS is used for the experimental determination of the parameters of the EFG tensor at copper sites, because aspherical valence electrons do not contribute to the EFG for a $^{67}Zn^{2+}$ probe; as a result, we have

$$eQU_{zz} \approx eQ(1 - \gamma)\, V_{zz}, \quad (2)$$

where U_{zz} and V_{zz} are the principal components of the total and crystal EFG tensors for $^{67}Zn^{2+}$, and γ is the Sternheimer coefficient of the Zn^{2+} ion.

However, even in the case of ^{67}Cu(^{67}Zn) EMS the number of experimentally measured parameters falls short of the number of charges to be determined, and auxiliary fitting parameters still need to be introduced [2]. In this light it is crucial to find general functional relations between ^{63}Cu NMR and ^{67}Cu(^{67}Zn) and ^{61}Cu(^{61}Ni) EMS data, thereby providing a means for qualitatively assessing the charge state of atoms in high-T_c superconductor lattices. In this article we establish such relations between the quadrupole interaction constants for the ^{63}Cu (C_{Cu}), ^{67}Zn (C_{Zn}), and ^{61}Ni (C_{Ni}) nuclei, and from a discussion of previously proposed [1] model distributions of the charge states of atoms in copper metal oxide lattices we identify these distributions.

2. Correlation between C_{Cu} and C_{Zn}

Fig. 1 summarizes experimental data obtained on $|C_{Cu}|$ and C_{Zn} for copper metal oxides both by the ^{63}Cu NMR method [1] and by the ^{67}Cu(^{67}Zn) EMS method [2]. We see that points corresponding to the divalent-copper compounds fit a straight line, where

$$C_{Cu} = 195 - 11\, C_{Zn}. \quad (3)$$

All quantities are given in megahertz.

It follows from relations (1) that the linear relation (3) is a consequence of the fact that the valence component of the EFG for Cu^{2+} is identical in the divalent-copper compounds.

The points for Cu_2O and $Nd_{1.85}Ce_{0.15}CuO_4$ and the Cu(l) sites in $YBa_2Cu_3O_6$ and $YBa_2Cu_3O_7$ are situated away from the line (3). At least two reasons account for this: 1) a deviation of the valence of copper from the standard +2 (copper in Cu_2O and copper at Cu(l) sites of the $YBa_2Cu_3O_6$ lattice are monovalent, whereas in $Nd_{1.85}Ce_{0.15}CuO_4$ the valence of copper differs

significantly from +2 [3]); 2) different orientations of the principal axes of the total and crystal EFG tensors (for $^{63}Cu(l)^{2+}$ centers in $YBa_2Cu_3O_6$ we have $U_{zz}=U_{bb}$ and $V_{zz} = V_{aa}$ [3]).

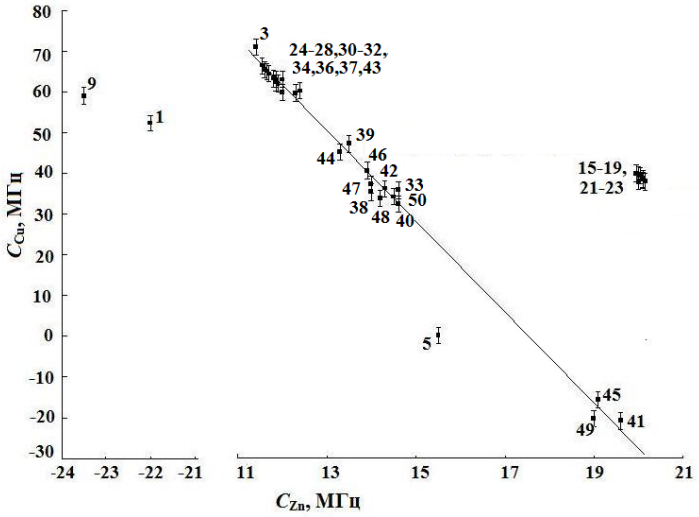

Fig. 1. |C(Cu)| — C(Zn) diagram for copper sites.
The straight line is the least squares fit through points corresponding to divalent copper.
The numbering of the points corresponds to Table

The numbering of the points in fig. 1–4

№	Lattice site	Coupling	№	Lattice site	Coupling
1	Cu	Cu_2O	26	Cu2	$SmBa_2Cu_3O_7$
2	Cu	CuO	27	Cu2	$EuBa_2Cu_3O_7$
3	Cu	$La_{1.85}Sr_{0.15}CuO_4$	28	Cu2	YBa_2Cu_3O7
4	Cu	La_2CuO_4	29	Cu2	$GdBa_2Cu_3O_7$
5	Cu	$Nd_{1.85}Ce_{0.15}CuO_4$	30	Cu2	$DyBa_2Cu_3O_7$
6	Cu	Nd_2CuO_4	31	Cu2	$HoBa2Cu_3O_7$
7	Cu1	$NdBa_2Cu_3O_6$	32	Cu2	$ErBa_2Cu_3O_7$
8	Cu1	$GdBa_2Cu_3O_6$	33	Cu2	$TmBa_2Cu_3O_7$
9	Cu1	$YBa_2Cu_3O_6$	34	Cu2	$YbBa_2Cu_3O_7$
10	Cu1	$YbBa_2Cu_3O_6$	35	Cu1	$SmBa_2Cu_4O_8$
11	Cu2	$NdBa_2Cu_3O_6$	36	Cu1	$YBa_2Cu_4O_8$
12	Cu2	$GdBa_2Cu_3O_6$	37	Cu1	$ErBa_2Cu_4O_8$
13	Cu2	$YBa_2Cu_3O_6$	38	Cu2	$SmBa_2Cu_4O_8$
14	Cu2	$YbBa_2Cu_3O_6$	39	Cu2	$YBa_2Cu_4O_8$
15	Cu1	$NdBa_2Cu_3O_7$	40	Cu2	$ErBa_2Cu_4O_8$
16	Cu1	$SmBa_2Cu_3O_7$	41	Cu1	$Y_2Ba_4Cu_7O_{15}$
17	Cu1	$EuBa_2Cu_3O_7$	42	Cu2	$Y_2Ba_4Cu_7O_{15}$
18	Cu1	YBa_2Cu_3O7	43	Cu3	$Y_2Ba_4Cu_7O_{15}$
19	Cu1	$GdBa_2Cu_3O_7$	44	Cu4	$Y_2Ba_4Cu_7O_{15}$
20	Cu1	$DyBa_2Cu_3O_7$	45	Cu	$Tl_2Ba_2CuO_6$
21	Cu1	$HoBa2Cu_3O_7$	46	Cu	$Tl_2Ba_2CaCu_2O_8$
22	Cu1	$ErBa_2Cu_3O_7$	47	Cu1	$Tl_2Ba_2Ca_2Cu_3O_{10}$
23	Cu1	$TmBa_2Cu_3O_7$	48	Cu2	$Tl_2Ba_2Ca_2Cu_3O_{10}$
24	Cu1	$YbBa_2Cu_3O_7$	49	Cu	$Bi_2Sr_2CuO_6$
25	Cu2	$NdBa_2Cu_3O_7$	50	Cu	$Bi_2Sr_2CaCu_2O_8$

3. Correlation between C_{Cu} and V_{zz}

The $C_{Cu} - V_{zz}$ diagram is analogous to the $|C_{Cu}| - C_{Zn}$ diagram, since C_{Zn}, according to (2), is proportional to V_{zz}, but contains a larger number of points, since the values of C_{Zn} have been measured for a limited number of oxides. We determine the sign of C_{Zn} from the $|C_{Cu}|$-C_{Zn} diagram as described above and, when this is not feasible, from a comparison of the orientations of the principal axes of the total, crystal, and valence EFG tensors.

It is evident from Fig. 2 that for a large part of the data the points of the $C_{Cu} - V_{zz}$ fit the straight line

$$C_{Cu} = 188 - 204\ V_{zz} \qquad (4)$$

As in Fig. 1, the points for Cu_2O, for Cu(l) in $YBa_2Cu_3O_6$ and $YBa_2Cu_3O_7$, and for $Nd_{1.85}Ce_{0.15}CuO_4$ deviate from the line (4) in Fig. 2. The causes of these deviations have already been discussed. More significant is the fact that the $C_{Cu} - V_{zz}$ discloses another reason for the deviation from the straight line (4): the incorrect value calculated for V_{zz}. This disclosure can be exploited to choose from several possible model charge distributions one that will satisfy relation (4). For an incorrect choice of model a point representing a give copper site is found on the line (3) in Fig. 1, but away from the line (4) in Fig. 2. From Figs. 1 and 2, it is evident that this situation occurs for Cu(1) sites in $YBa_2Cu_4O_8$ and $Y_2Ba_4Cu_7O_{15}$. Figure 2 shows that the calculated value of V_{zz} is somewhat too large for Cu(1). This fact underscores the need to introduce modifications in proposed earlier model for the charge distribution among the sites of $YBa_2Cu_4O_8$ and $Y_2Ba_4Cu_7O_{15}$.

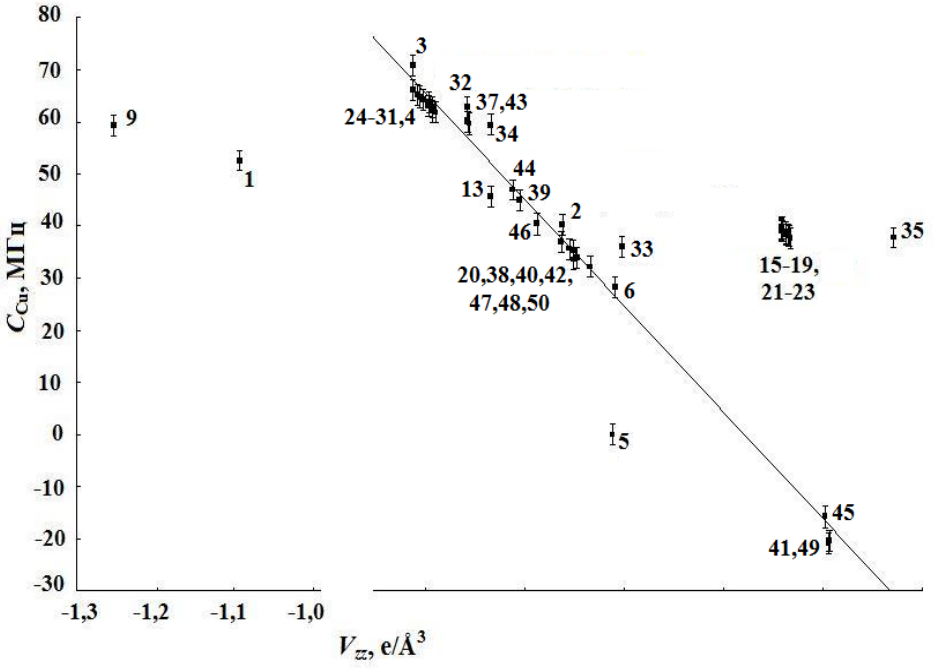

Fig. 2. C(Cu) − V_{zz} diagram for copper lattice sites.
The straight line is the least squares fit through points 1–13 corresponding to divalent copper.
The numbering of the points corresponds to Table

4. Correlations between C_{Ni} and V_{zz} and C_{Ni} and C_{Zn}

Figs. 3, 4 present a C_{Ni} vs. V_{zz} and C_{Ni} vs. C_{Zn} graphs for the divalent-copper compounds. The quadrupole coupling constant C_{Ni} was measured for the ^{61}Ni probe in cuprous oxides by EMS [2]. It is readily seen that the experimental points fit straight lines

$$C_{Ni} = -80 + 48\ V_{zz} \quad (5)$$

for $C_{Ni} - V_{zz}$ diagram and

$$C_{Ni} = -79 + 2\ C_{Zn} \quad (6)$$

for $C_{Ni} - C_{Zn}$ diagram.

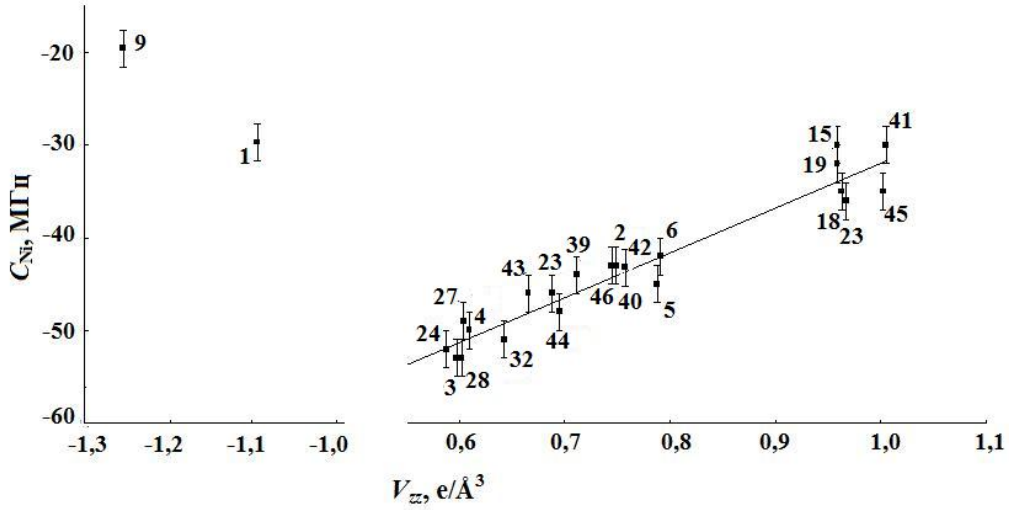

Fig. 3. $C_{Ni} - V_{zz}$ diagram for copper lattice sites. The straight line is the least squares fit through points corresponding to divalent copper. The numbering of the points corresponds to Table

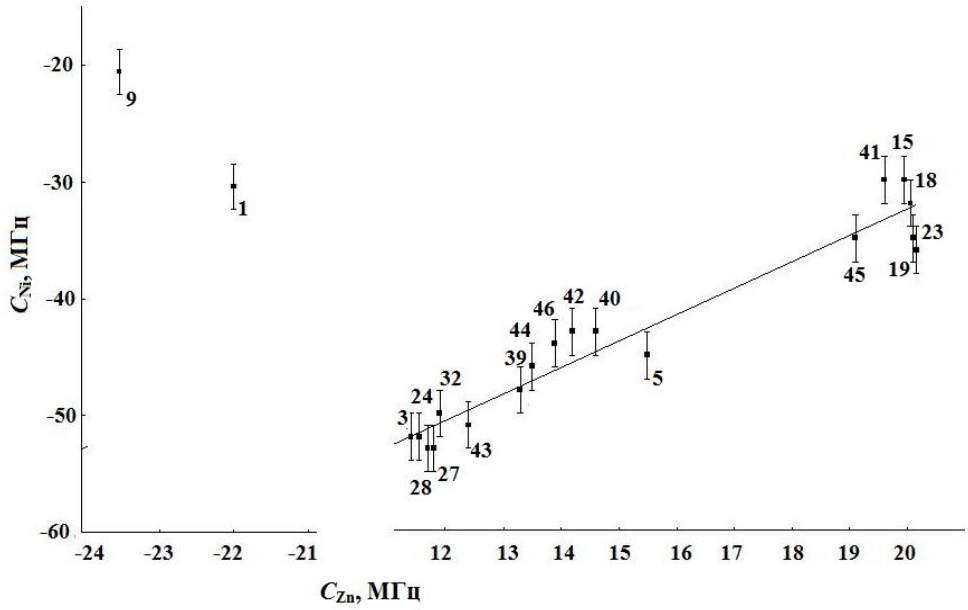

Fig. 4. $C_{Ni} - C_{Zn}$ diagram for copper lattice sites.
The straight line is the least squares fit through points corresponding to divalent copper.
The numbering of the points corresponds to Table

As in Figs. 3 and 4, the points for Cu_2O, for Cu(l) in $YBa_2Cu_3O_6$ deviate from the lines (5) and (6). The reasons of these deviations have already been discussed. It follows from relations (1) and (2) that the linear relations (5) and (6) are a consequence of the fact that the valence component of the EFG for Ni^{2+} is identical in the divalent-copper compounds.

Thus, using diagrams $C_{Ni} - V_{zz}$ and $C_{Ni} - C_{Zn}$ the divalent-copper compounds can be selected. The $|C_{Cu}| - C_{Zn}$ diagram is therefore used to select such copper centers without invoking any kind of model.

5. Correlation between C_{Cu} and C_{Ni}

Fig. 5 presents a C_{Cu} vs. C_{Ni} graph for the divalent-copper compounds. It is readily seen that the experimental points fit a straight line

$$C_{Cu} = -193 - 5\, C_{Cu}, \qquad (7)$$

This linear dependence can be understood if we recall that the EFG at nucleus sites for the Ni^{2+} and Cu^{2+} centers is generated both by the lattice ions (the crystal field EFG) and by the nonspherical valence shell of the ion itself (the valence EFG), so the quadrupole coupling constant for the probe can be cast as relation (1).

The linear relation |C(Ni)| vs. |C(Cu)| is actually a consequence of the linear relations C(Ni) vs. V_{zz} and C(Cu) vs. V_{zz}, which were observed for compounds of divalent copper. Since the data obtained for the Cu(2) sites in the $RBa_2Cu_3O_7$ and $RBa_2Cu_3O_6$ compounds are on the straight line, one may conclude that copper in these sites is in the divalent state.

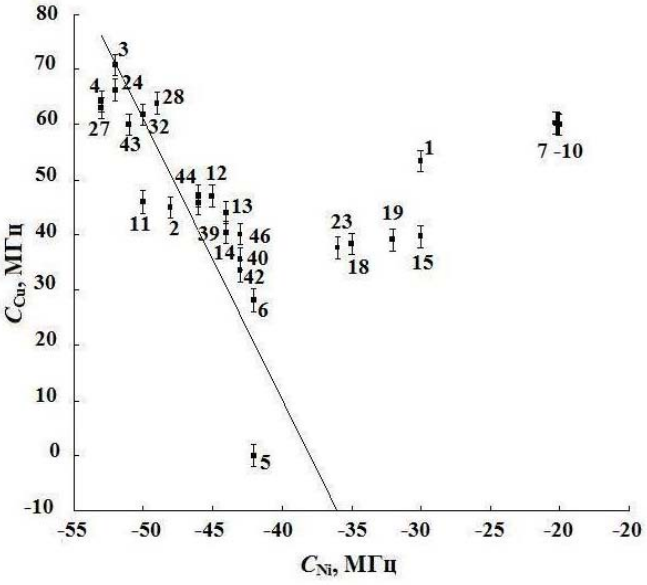

Fig. 5. $C_{Cu} - C_{Ni}$ diagram for copper lattice sites. The straight line is the least squares fit through points corresponding to divalent copper. The numbering of the points corresponds to Table

From fig. 5 it is seen that the points obtained for the copper sites in Cu_2O and for the Cu(1) sites in $RBa_2Cu_3O_6$ and $RBa_2Cu_3O_7$ deviate from a linear relationship. There are two reasons for this deviation, namely, the copper valence state being other than 2+ and different orientations of the total and valence EFG axes for the $^{61}Ni^{2+}$ and $^{63}Cu^{2+}$ probes. The first reason is valid for the Cu(1) sites in $RBa_2Cu_3O_6$ and for the copper sites in Cu_2O [the copper in Cu_2O and in the Cu(1) sites of the $RBa_2Cu_3O_6$ compounds is univalent], and the second applies to the Cu(1) sites in the $RBa_2Cu_3O_7$ compounds (it is known that, at least for the Cu(1) sites in $YBa_2Cu_3O_7$, the z axis of the total EFG tensor is directed along the b crystallographic axis, whereas the z axis of the crystal-field EFG is aligned with the a crystallographic axis).

The $C_{Ni} - C_{Cu}$ diagram is therefore used to select such copper centers without invoking any kind of model.

6. Conclusion

Thus, a linear relation between C_{Cu} (^{63}Cu NMR data) and C_{Zn} and C_{Ni} (^{67}Cu(^{67}Zn) and ^{61}Cu(^{61}Ni) EMS data) holds for the majority of metal oxides of divalent copper, indicating the similarity of the electronic structure of copper (Cu^{2+}, $3d^9$) in these lattices. The data for copper in Cu_2O and for copper at Cu(l) sites of the $YBa_2Cu_3O_6$ are naturally excluded from this relation [owing to the monovalence of the copper (Cu^+, $3d^{10}$) in these lattices], as are the data for Cu(l) in $YBa_2Cu_3O_7$ (since the principal axes of the total and crystal EFG have different orientations). An analogous linear relation obtains between C_{Cu} (^{63}Cu NMR data) and V_{zz} (calculated in the approximation of the point-charge model) for a much larger number of metal oxides of copper except the already mentioned ones. The latter relation can be used to assess the validity of proposed model charge distributions among the lattice sites for superconducting ceramics.

References

1. *Asayama K., Kitaoka Y., Zheng G.-Q., Ishida K., Magishi K.* NMR study of high-TC superconductors // Physica B: Condensed Matter. 1996. V. 223–224. № 1–4. P. 478–483.

2. *Bordovsky G., Marchenko A.,* and *Seregin P.* Mössbauer of Negative Centers in Semiconductors and Superconductors. Identification, Properties, and Applicaton. Academic Publishing GmbH & Co. 2012. 499 p.

3. *Seregin P. P., Masterov V. F., Nasredinov F. S., Seregin N. P.* Correlations of the ^{63}Cu NQR/NMR data with the ^{67}Cu(^{67}Zn) emission Mössbauer data for htsc lattices as a tool for the determination of atomic charges // Physica Status Solidi (B): Basic Solid State Physics. 1997. V. 201. No. 1. P. 269–275.

А. В. Ляпцев

СИММЕТРИЯ В ЗАДАЧАХ НЕЛИНЕЙНОЙ ДИНАМИКИ. ПРОЯВЛЕНИЕ СВОЙСТВ СИММЕТРИИ В ПОЛЯРИЗАЦИИ ИЗЛУЧЕНИЯ

Исследовано проявление свойств симметрии хаотического движения в случае, когда система описывается уравнениями классической динамики, а точечная группа симметрии системы содержит некоммутирующие элементы и, как следствие, имеет двумерные неприводимые представления. Численными расчетами показано, что излучение такой системы полностью деполяризовано, в то время как при понижении симметрии системы излучение становится частично поляризованным. Такие поляризационные характеристики полностью соответствуют характеристикам, получаемым при квантово-механическом описании аналогичной системы.

Ключевые слова: нелинейная динамика, динамический хаос, симметрия, поляризация излучения.

A. Liaptcev

Symmetry in Problems of Nonlinear Dynamics. The Manifestation of The Properties of The Symmetry in The Polarization of Radiation

Manifestation of symmetry properties of chaotic motions is investigated in a case when the system is described by equations of classical dynamics. The considered group of symmetry contains non-commuting elements and as consequence has two-dimensional irreducible representations. Numerical calculation shows, that radiation of this system are fully depolarized, at the same time at a lower symmetry of the system, radiation becomes partially polarized. Such